Advanced Powder Technology (2013). 24(5), 864-870.
DOI: http://dx.doi.org/10.1016/j.apt.2013.03.011

TEM–STEM study of europium doped gadolinium oxide nanoparticles synthesized by spray pyrolysis

L.S. Gomez-Villalba [b], E. Sourty [c], B. Freitag [c], O. Milosevic [d], M.E. Rabanal [a,*]

[a] Universidad Carlos III de Madrid and IAAB, Materials Science Department, Avda de la Universidad 30, 28911-Leganés, Madrid, Spain
[b] Instituto de Geociencias (CSIC, UCM), C/Jose Antonio Novais 2, 28040-Madrid, Spain
[c] Applications Laboratory FEI Company, Eindhoven, The Netherlands
[d] Institute of Technical Sciences of the Serbian Academy of Sciences and Arts, K. Mihajlova 35/IV, 11000 Belgrade, Serbia
* Corresponding author. E-mail addresses: luzgomez@geo.ucm.es (L.S. Gomez-Villalba), eugenia@ing.uc3m.es (M.E. Rabanal).

Abstract: Scanning-Transmission and Transmission Electron Microscopy techniques (STEM and TEM) have been applied to the characterization of nanostructured gadolinium oxides doped with europium synthesized by spray pyrolysis. The High Angle Annular Dark Field (HAADF) – Scanning Transmission Electron Micros-copy (STEM) tools have been used to perform a tomographic study to identify morphological character-istics of nanostructured particles, and to differentiate them according to the heat treatments to which these have been subjected. With these techniques it has been possible to confirm the hollowness and por-ous nature of samples subjected to low temperature annealing (900 °C). Moreover, the beginning of the densification and sintering processes in samples subjected to thermal treatment at higher temperature (1100 °C) have been evaluated. Chemical analysis by electron energy loss spectroscopy (EELS) and X ray energy dispersive spectroscopy (EDS) carried out in STEM mode have allowed to confirm the high uni-formity and the expected chemical composition. The high resolution tools either allowed to confirm the presence of a cubic (Ia3 symmetry) and the monoclinic (c2/m symmetry) phases in the nanostructured particles.

Keywords: Nanostructure, Electron microscopy (STEM, TEM), Tomography, Electron energy loss spectroscopy (EELS), Spray pyrolysis

1. Introduction

The development of several *bottom up* synthesis methods, in recent years, has stemmed from the increasing interest in obtaining nanostructured particles with improved properties. Of these methods, the so-called Spray Pyrolysis (SP) is arguably one the most useful [1]; this method enables the production of non-agglomerated spherical particles with a large surface area and narrow particle size distribution [2]. A precursor solution is atomized producing fine droplets that are transported to a high temperature reactor. Several processes occur, including solvent evaporation, solute diffusion, droplets drying, precipitation, and reactions between the precursor/gas [1,2]. Depending on the atomizing technique, processing parameters (carrier gas flow rate, residence time, decomposition temperature) and physicochemical properties of the precursor solution (concentration, pH, surface tension, viscosity) lead to obtain particles ranging from few nanometers to several micrometers [3]. Several authors [4,5] have focused on the formation and growth mechanism of nanoparticles. This process involves the nucleation, growth and aggregation of primary nanoparticles leading to the formation of a spherical assemblage of secondary particles. Among the different application requirements, the objectives are mainly focused on making hollow or filled particles with rough or smooth surfaces [4].

Many progresses in the field of nanostructured ceramic materials with functional applications depend on the particle morphology, structure and composition. These properties are highly sensitive to the specific aspects of particle geometry, local crystal structure or variations in the chemical composition. Most research, however, has been undertaken using characterization techniques mainly based in conventional Scanning Electron Microscopy (SEM) or Transmission Electron Microscopy (TEM). However, characteristics such as the porosity or roughness of nanoparticles require the use of specific tools.

The advances in nanotechnology related to the decrease of the particle size and improvement of their functional properties also bring new challenges for materials characterization and defect analyses [6]. These include surface roughness measurements, characterization of defects or understanding three dimensional (3D) geometries [7,8]. The characterization of the 3D structure is essential to understand the morphology of materials [9]. The method of 3D tomography is based on the processing of images which are ta-

ken in sections using penetrating waves. This maximizes the viewing directions, allows the internal structure of to be observed and can provide quantitative 3D information on material characteristics [10].

The 3D image is the volumetric reconstruction of an object from many sequential views; with each view the angle of incidence with respect to the sample surface is varied [11]. This approach was first successfully applied in the field of life sciences [12,13]. In materials science, nanoscale tomography is a vibrant and multifaceted research field that is currently in a period of rapid development. It provides important material information on surface analysis, for example, the porosity or geometry of materials [14].

The use of HRTEM, HRSTEM and electron diffraction in combination with highly sensitive spectroscopic techniques (EELS–EDS) provides insights into the relationship between microscopic structure, chemical variations and functional properties with greater ease. EDS can give elemental information and EELS, on the other hand, can not only give elemental information but can also be used to obtain information on chemical and physical properties [14].

In the present study, the goal was to carry out a detailed characterization that contributes to understand the growing mechanisms during SP. The three characterization tools addressed were morphology, structure and chemical composition. The morphology was studied using the tomography by STEM. The chemical analysis was studied using two complementary techniques, EELS and EDS. Finally, the structural control was assessed by combining high resolution techniques (HRTEM, HRSTEM) and electron diffraction.

The characterization was carried out over nanoparticles of rare earth oxides of Gadolinium doped with Europium synthesized by SP. Gadolinium or Yttrium doped with Europium oxides are important due to their luminescent properties [15,16]. Higher luminescence efficiency and long-term stability of this material are mostly associated with investigating optimum doping concentration, nanostructuring and obtaining overall morphology control. In comparison to phosphor particles obtained by conventional methods that have micron-sized grains and irregular morphologies, the use of fine submicronic spherical particles increases the screen brightness and improves the resolution because of lower scattering of light and higher packing densities [17,18]. It is evident that the control over morphology and size; stoichiometry and composition; and surface characteristics must be established during synthesis process in order to obtain the desirable objectives of improved powder phosphors [19].

Both the morphology and structure affect the quality of their luminescent properties. Luminescence studies carried out in Gd_2O_3:Eu^{3+} phosphor system have demonstrated that annealing and crystalline phases control both the thermoluminescence and radioluminescence signals [15]. Characteristic bands in the emission spectra are assigned to Eu^{3+} ion radiative $^5D_0 \rightarrow {}^7F_i$ ($i = 0,1,2,3,4$) transitions. In all the samples maximum intensity peak is at 611 nm wavelength belonging to $^5D_0 \rightarrow {}^7F_2$ transition [20]. All observed transitions are due to the Eu^{3+} in C2 and S6 crystallographic sites. In Y_2O_3:Eu, the lifetime measurements revealed the quenching effect with the rise of dopant concentration and its more consistent distribution into host lattice due to the thermal treatment [16]. However, there are currently a number of doubts concerning the specific morphological characteristics (roughness, porosity) that affect the quality of the luminescent response. Here, Gd_2O_3:Eu^{3+} phosphors were obtained through spray pyrolysis from pure nitrate solution. Host gadolinium/yttrium oxides exhibit two polymorphic forms, cubic (low temperature) and monoclinic (high temperature) structures [21,22]. This paper aims to provide the results from new techniques to clarify in detail the morphological, chemical and structural aspects related to the synthesis and post-treatments performed by the SP method.

2. Materials and methods

2.1. Powder processing

Powder samples were prepared by the SP method from water solution of $Gd(NO_3)_3{\cdot}6H_2O$ and $Eu(NO_3)_3{\cdot}5H_2O$ as precursors in order to obtain "as-prepared" particles having 0.07/0.03 Gd-to-Eu molar ratio. The common water solution (0.1 mol dm^{-3}) was ultrasonically atomized with a device working at 2.1 MHz and subsequently decomposed in a high-temperature tubular flow reactor (length 1.6 m, radio 22×10^{-3} m) at 700 °C. Dried air was used as a carrier gas (flow rate 2.5×10^{-5} m^3/s). The drop velocity was 0.00657 m/s in order to obtain a residence time in the entire tube of 24.33 s and a residence time in the reaction zone of 7.6 s. Samples were subjected to post thermal treatments in air atmosphere at 900 °C (nn-900) and 1100 °C (nn-1100) for 12 h.

2.2. Microscopic characterization

The tomographic study was conducted over two representative samples annealed at 900 °C and 1100 °C/12 h. The tilt-series were automatically acquired on a TEM Tecnai G2 F20 X-Twin (FEI Company) used in STEM mode with a Fischione model 3000 HAADF detector for Z contrast imaging. A Fischione single-tilt tomography holder with a maximum tilt range of ±80° was used. Samples were tilted around the a-tilt axis of the goniometer from −76° to +76° at regular intervals of 2°. This minimizes artifacts due to the limited tilt range during acquisition known as missing-wedge artifacts (part of the tilt-range not covered during the tilt-series acquisition) [23].

Seventy-seven micrographs 1024×1024 pixels in size were acquired automatically at a nominal magnification of 160.000 times. The magnification typically corresponds to a pixel size of 1.6 nm^2 with a field of view of 1.64 μm^2 and voxel size of 1.6 nm^3 Alignment was done using cross correlation between successive images in the tilt series, sequentially compensating for image shifts through the entire tilt series, thus making marker tracking unnecessary [8]. After that, the alignment of the 3D volume was reconstructed using iterative weighted back projection [24]. The simultaneous iterative reconstruction algorithm (SIRT) [23] with 15 interactions using Inspect 3D v 2.5 X press edition software suite (FEI Company) and the Resolve RT (Mercury Computer Systems, FEI edition) software have been used for visualization and rendering.

The structural and chemical characterization was carried out in a TEM Titan 80-300™ operated at 300 kV combined with selected area electron diffraction (SAED). Chemical composition was assessed by line scan EDS–STEM and STEM–EELS.

3. Results and discussion

3.1. Morphological analysis

The conventional TEM in bright field mode (Fig. 1a) allows identification of spherical and disaggregated nanoparticles (78–500 nm) in the sample after a thermal treatment at 900 °C/12 h. However, the HAADF–STEM mode (Fig. 1c) suggests a porous surface as revealed by contrast. Visual inspection of the tilt series (HAADF–STEM, Fig. 1b) allows identification of bright and dark areas in a spherical particle (500 nm). Dark contrast observed in the tilt series indicates the presence of voids (between 44 and 200 nm), and rough particle surfaces. The reconstructed images (Fig. 1d) with enhanced contrast confirm porous and rough surfaces. The particle cross-section (Fig. 1e) indicates the presence of a crust on the particle surface with pores on the external shell.

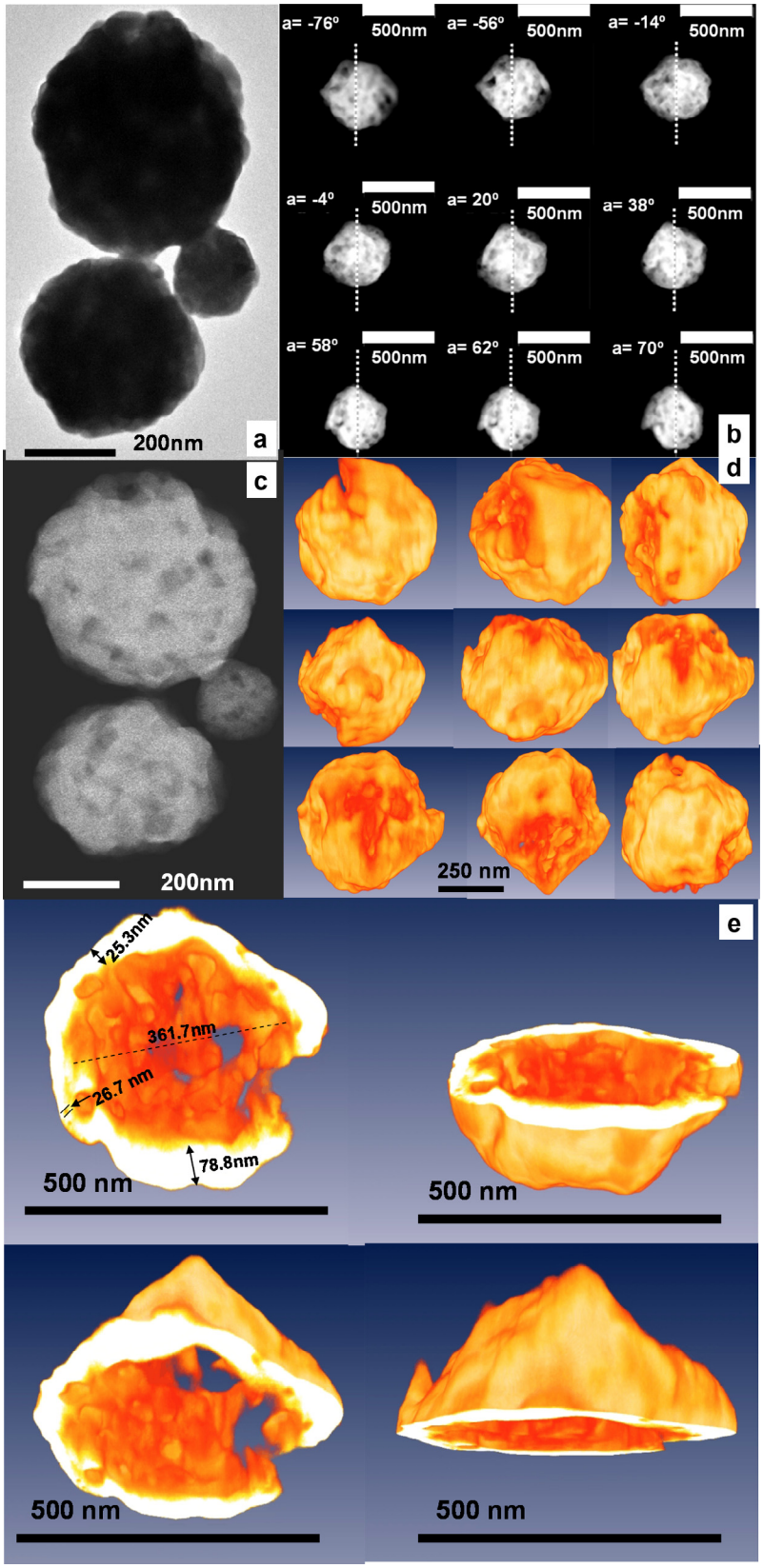

Fig. 1. TEM and STEM images of the nn-900 sample. Conventional TEM image in bright field mode (a), Visual inspection of the tilt series in HAADF–STEM mode (b). HAADF-STEM image (c). Reconstructed images of the tilt series (d). Details of the reconstructed cross section (e).

It shows a difference in thickness of the crust (25–78 nm). These results confirm the hollowness observed in the reconstructed images. The crust formation, particle hollowness and pores result from the concentration/temperature gradient formed at the droplet level in the evaporation/drying stage. These mainly depend on the solute concentration/properties and the processing parameters [3,25]. During the evaporation/drying period, the temperature difference between the droplet surface and the interior leads to the

formation of a concentration gradient. It causes faster evaporation from the droplet surface than solvent diffusion towards the surface. The prevailing surface precipitation consequently leads to the formation of a crust. This crust prevents further solvent diffusion and leads to an increase in pressure inside the dried particles and shell porosity. Particle roughness is presumably a consequence of the crystallization of the primary particles, whereas aggregation and growth of the secondary particles are

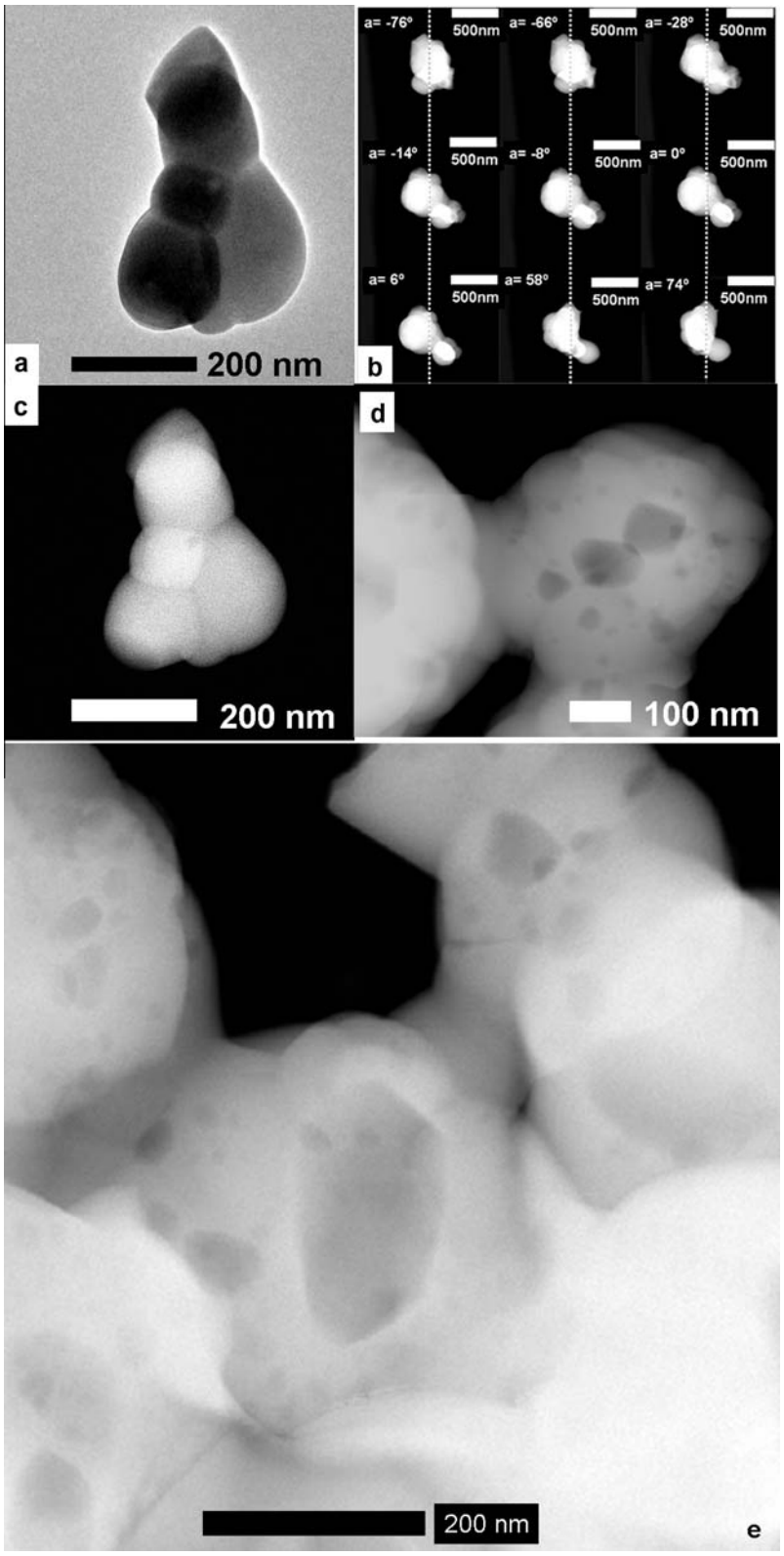

Fig. 2. TEM and STEM Images of the nn-1100 sample. Conventional TEM image in bright field mode (a). Visual inspection of the tilt series in HAADF–STEM mode (b). HAADF–STEM image (c). Details of one HAADF–STEM image showing the inter and intra particular porosity (d and e).

caused by the temperature increase [1,21]. STEM–HAADF results confirm the presence of non-agglomerated spherical particles produced after a low temperature thermal treatment (nn-900 – Fig. 1) indicating high content of surface porosity.

With the temperature increase (1100 °C – Fig. 2), the beginning of the particle aggregation and initial stage of the sintering process are evident. The porous particle surface still persists implying the lack of particle densification even at increased temperature and for reasonable time (12 h). The observations carried out in the higher temperature sample shows that increasing the annealing temperature causes interparticle collision and sintering among the particles (Tem image Fig. 2a, STEM image Fig. 2c). The tomography tilt-series (Fig. 2b) shows further particle densification, a decrease in porosity and more agglomeration among the particles. Both inter- and intra-particle sintering occurs among the particles – this affects the particle morphology (Fig. 2d and e).

3.2. Chemical results

Chemical information about the local atom coordination is obtained from EELS spectra. Fig. 3a shows a HAADF–STEM image of the sample with Gd/Eu: 0.07/0.03 M ratio heated at 900 °C. The line

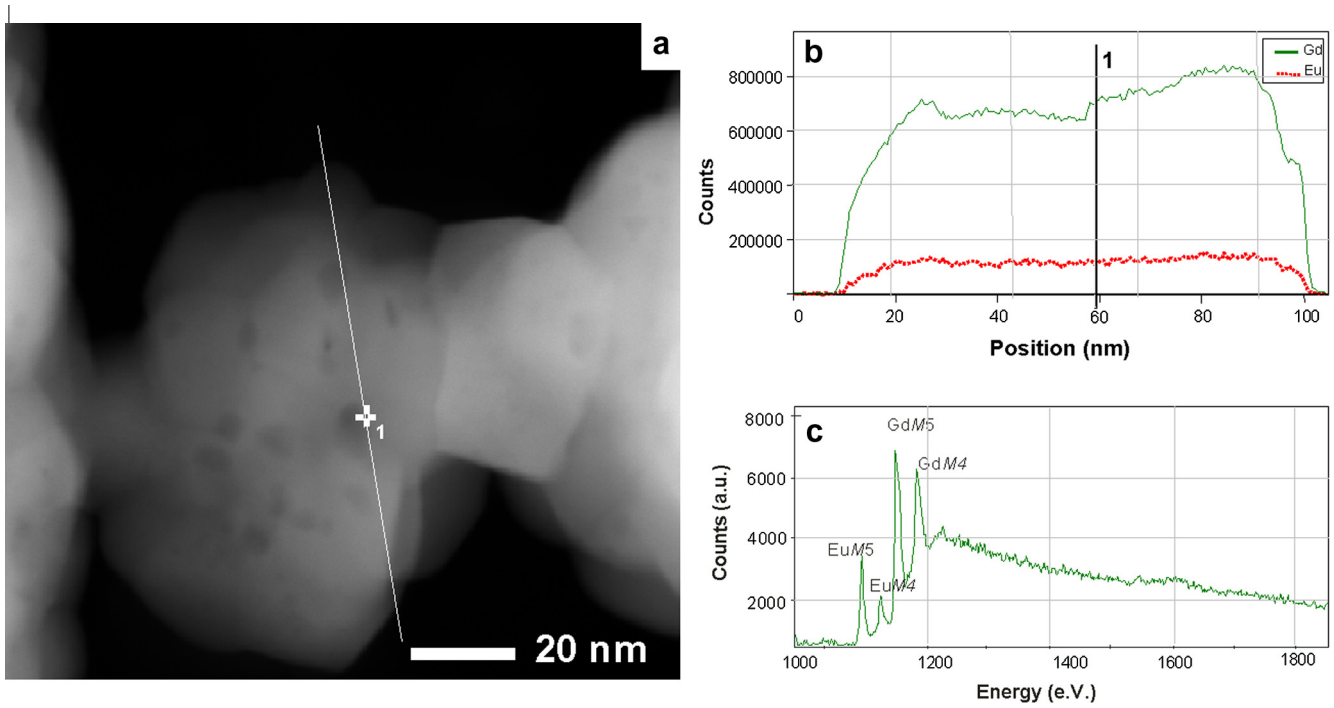

Fig. 3. HAADF–STEM image of the sample with Gd/Eu: 0.07/0.03 M ratio heated at 900 °C (a). Line profile of the Gd/Eu ratio (b), EELS spectrum (c).

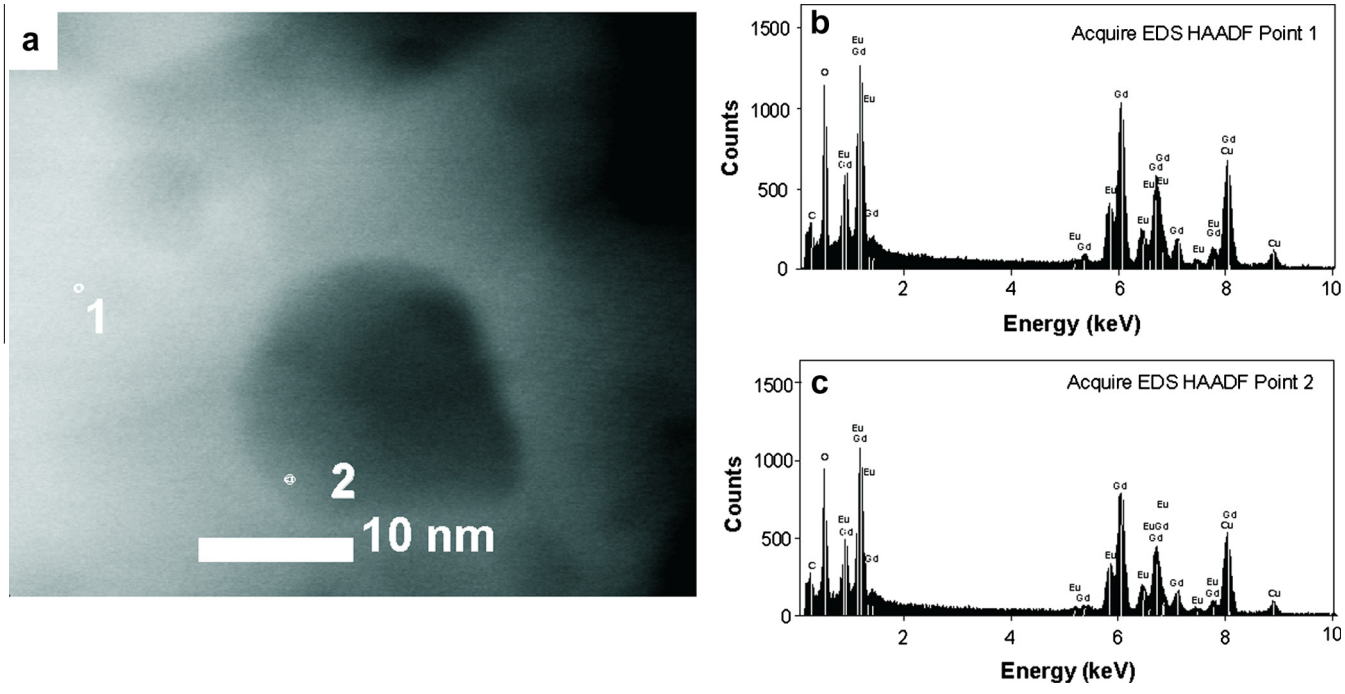

Fig. 4. STEM images of the sample after a thermal treatment at 900 °C (a), EDS results (b and c) taken along a line scan.

(0–100 nm) indicates the direction of the sequence of acquisition of the EELS spectrum. The line profile (Fig. 3b) shows that the ratio between the Gd/Eu remains constant indicating a homogeneous mixture of the elements in the particles. The spectrum (Fig. 3c) has been taken in the area delineated with a cross (point 1). There are two prominent signals, equivalent to the 3d electron transition to the 4f empty states (*M*5: 3d5/2 → 4F7/2, *M*4, 3D3/2 → 4F5/2) [26,27]. Normally, the energy loss spectra of the rare earths are characterized by sharp *M*4,5 edges [28]. The Energy Loss Near Edge Spectrum (ELNES) confirms the signals of Eu in the *M*5 (∼1129–1140 eV) and Eu *M*4 (∼1158–1169 eV) edges, and the Gd in its *M*5 (∼1182–1198 eV) and *M*4 (∼1215–1230 eV M4) edges respectively. With the ELNES information it is possible to obtain information about the local atom coordination. The *M*4/*M*5 ratio is normally calculated to establish the oxidation state. Measurements made on different particles allow the determination of the *M*4/*M*5 relationship, which varies between 0.83 and 0.9. These values are in the range observed for rare earth indicating a 3^+ oxidation state [29]. These results confirm previous studies carried out by EELS–EFTEM [30]. The atomic contrast provided by STEM shows darker and brighter regions in the particles (Fig. 4a). The EDS measurements confirm that the contrast change is not a result of changes in chemical composition but is that it is instead due to the porosity of the material. The EDS results (Fig. 4b and c) taken along a line scan in the nn-900 particle confirm the uniform distribution of the Eu in the gadolinia matrix. This leads to the conclusion that the distribution of the Gd/Eu ratio is also uniform. EDS also confirms the same Gd/Eu ratio both for the darker and brighter contrast regions. A small signal of Cu comes from the copper grid. Semi-quantitative EDS-STEM results provide the Gd/Eu atomic ratio (Gd – 73 at.%, Eu – 27 at.%) which is in accordance with the precursor solution nominal value (Gd – 70 at.%, Eu – 30 at.%).

3.3. Structural analysis

Structurally, both the HRTEM and HRSTEM taken in the nn-900 sample confirm the presence of crystalline domains of both cubic (Fig. 5a and c) and monoclinic (Fig. 5d) phases. The Ia3 cubic phase is confirmed in the TEM image (Fig. 5a) showing the (002) atomic distances, and also in the corresponding electron diffraction pattern (as inset) oriented along the [100] zone axis. The scattering of the HAADF–HRSTEM image (Fig. 5c) provides different intensity contrast. The (022) and (222) atomic planes are resolved. The corresponding fast fourier transformed (*fft*, as inset) confirms the [110] direction of the Ia3 phase. The existence of the monoclinic phase (Fig. 5d) is observed by HRTEM. The (002) and (110) atomic planes along the [220] zone axis with the corresponding *fft* (shown as inset) are in agreement with the c2/m phase. Changes in the

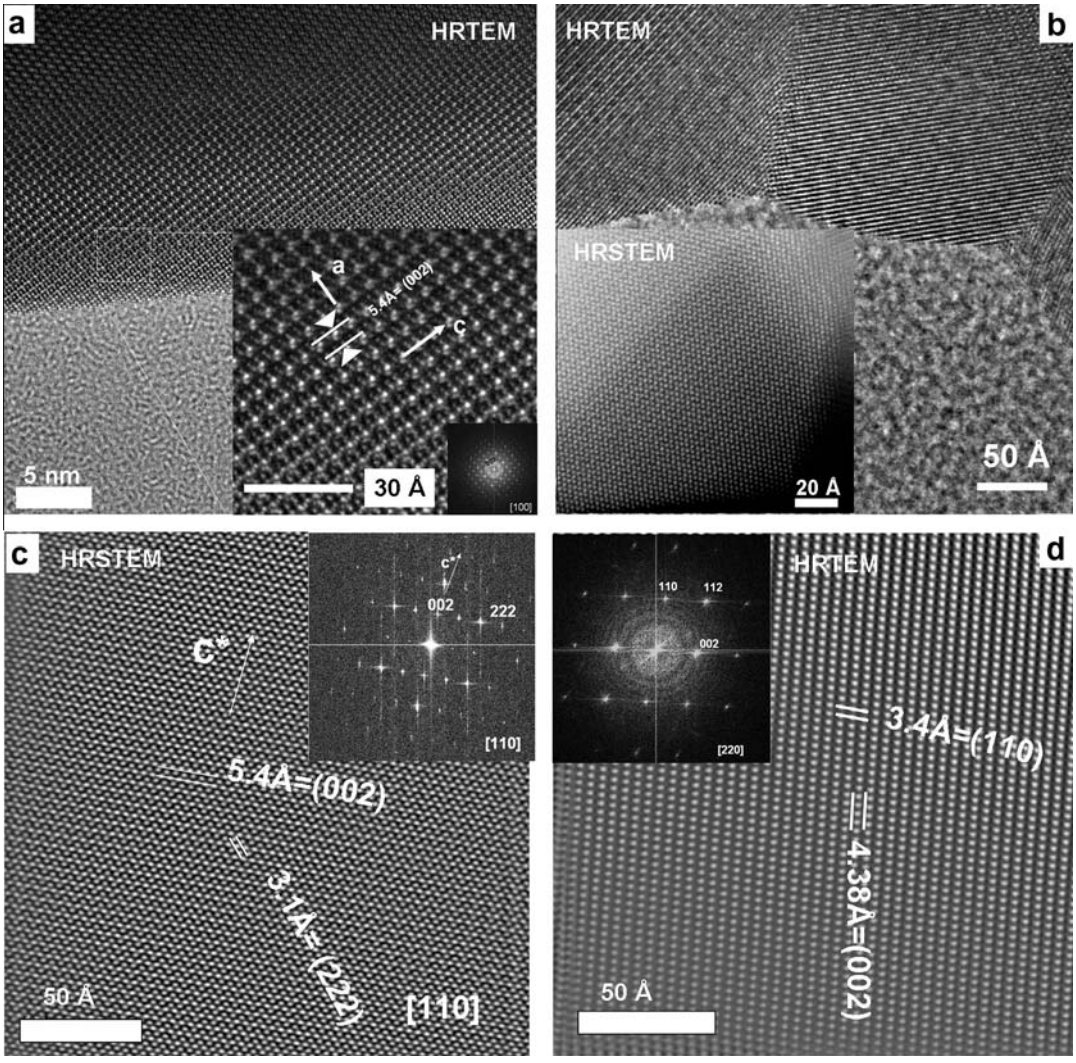

Fig. 5. HRSTEM and HRTEM images of the nn-900 sample. The cubic phase along the [100] zone axis (HRTEM- electron diffraction, (a) and [110] orientation (HRSTEM-*fft* (c). The monoclinic phase along the [220] zone axis, (HRTEM, *fft*, d). Crystalline domains observed by HRTEM and HRSTEM (b).

atomic plane orientation and local boundaries between the crystallites (HRTEM – Fig. 5b and HRSTEM – Fig. 5b as inset) enable definition of the crystalline domains.

4. Conclusions

In view of the results, some relevant aspects of the nanoparticles synthesized by SP and the subsequent heat treatments have been obtained. The use of STEM-tomography techniques have clarified some morphological aspects related to the synthesis and post thermal treatments. Given the synthesis conditions applied, it was possible to determine that the nanoparticles subjected to heat treatment to 900 °C/12 h kept their spherical morphology being hollow, rough and porous. These conditions change with a heat treatment at a higher temperature. It is confirmed that at 1100 °C/12 h particles tend to agglomerate, become denser and less porous. HRTEM images, HRSTEM and electron diffraction confirm the presence of the Ia3 cubic and the c2/m monoclinic phases. Also, the STEM–EDS technique has confirmed that the particles are chemically homogeneous. The STEM–EELS tool provides information about the oxidation state confirming the 3^+ for both the Gd and Eu.

It is expected that the results obtained here provide a basis for users of SP synthesis technique to establish a new routine for the morphological, chemical and structural characterization. Likewise, it is expected that the experimental conditions that have been used be useful to tailor nanoparticles with desired characteristics.

Acknowledgements

This work has been supported by the Advanced Structural Materials Program- ESTRUMAT (S2009/MAT-1585) and MAT2010-19837-C06-05. Thanks are extended to NanoPort (FEI)- Eindhoven, especially to Eng. L. Fernando Mendoza and to the Ministry of Science and Technology of Serbia (Project #142010). Thanks to Daniel McAllister for the English revision.

References

[1] K. Okuyama, I.W. Lenggoro, Preparation of nanoparticles via spray route, Chem. Eng. Sci. 58 (2003) 537–547.
[2] O. Milosevic, L. Mancic, M.E. Rabanal, L.S. Gomez, K. Marinkovic, Aerosol route in processing of nanostructured functional materials, Kona Powder Part. J. 27 (2009) 84–106.
[3] S. Che, O. Sakurai, K. Shinozaki, N. Mizutani, Structure control through intraparticle reactions by spray pyrolysis, J. Aerosol Sci. 29 (3) (1998) 271–278.
[4] G. Messing, SCh. Zhang, G. Jayanthi, Ceramic powder synthesis by spray pyrolysis, J. Am. Ceram. Soc. 76 (11) (1993) 2707–2726.
[5] S.H. Ju, Y.C. Kang, Effect of preparation temperature on the morphology, crystal structure and electrochemical properties of LiV_3O_8 powders prepared by spray pyrolysis, Mater. Chem. Phys. 126 (2011) 133–137.
[6] P.A. Midgley, M. Weyland, 3D electron microscopy in the physical sciences: the development of Z contrast and EFTEM tomography, Ultramicroscopy 96 (3–4) (2003) 413–431.
[7] P.D. Nellist, E.C. Cosgriff, G. Behan, Prospects for 3D characterization of materials by aberration corrected STEM and SCEM, Microsc. Microanal. 13 (2) (2007) 130–131.
[8] K. Kaneko, W.J. Moon, K. Inoke, Z. Horita, S. Ohara, T. Adschiri, H. Abe, M. Naito, Characterization of TiO_2–Ag nanocomposite particles prepared by spray pyrolysis process using transmission electron microscopy and three-dimensional electron tomography, Mater. Sci. Eng. A 403 (1–2) (2005) 32–36.
[9] C. Kübel, A. Voight, R. Schoenmakers, M. Otten, D. Su, T.C. Lee, A. Carlsson, H. Engelmann, J. Bradley, Recent advances in electron tomography: TEM and HAADF–STEM tomography for materials science and IC applications, Microsc. Microanal. 11 (5) (2005) 1–60.
[10] O. Ersen, C. Hirlimanna, M. Drillona, J. Werckmanna, F. Tihayb, C. Pham-Huuc, C. Crucifixd, P. Schultz, Characterization of nanometric objects, Solid State Sci. 9 (12) (2007) 1088–1098.
[11] G. Möbus, B.J. Inkson, Nanoscale tomography in materials science, Mater. Today 10 (12) (2007) 18–25.
[12] RA. Crowther, Procedures for three-dimensional reconstruction of spherical viruses by Fourier synthesis from electron micrographs, Philos. Trans. R. Soc. 261 (837) (1971) 221–230.
[13] B.L. Armbruster, J. Brink, M. Kawasaki, T. Isabell, R. O'Donnell, M. Kersker, Advances and challenges in electron tomography, Microsc. Microanal. 13 (2007) 1336–1337.
[14] D. Peacor, Analytical electron microscopy: X ray analysis, in: P. Buseck (Ed.), Minerals and Reactions at the Atomic Scale: Reviews in Mineralogy Transmission Electron Microscopy, vol. 27, Mineralogical Society of America, Washington, DC, 1992, pp. 112–180.
[15] Y. Wang Y, O. Milosevic, LS. Gómez, ME. Rabanal, JM. Torralba, B. Yang, PD. Towsend, Thermoluminescence responses from europium doped gadolinium oxide, J. Phys. Condens. Matter 18 (40) (2006) 9257–9272.
[16] K. Marinkovic, L. Mancic, L.S. Gomez, M.E. Rabanal, M. Dramicanin, O. Milosevic, Photoluminescense properties of nanostructured Y_2O_3:Eu^{3+} and $(Y_{1-x}Gdx)2O_3$:Eu^{3+} powder obtained by aerosol synthesis, Opt. Mater. 32 (12) (2010) 1606–1611.
[17] S.H. Byeon, M.G. Ko, J.C. Park, D.K. Kim, Low-temperature crystallization and highly enhaced photoluminescence of $Gd_{2-z}xYxO_3$:Eu^{+3} by li doping, Chem. Mater. 14 (2002) 603–608.
[18] Y.C. Kang, I.W. Lenggoro, S.B. Park, K. Okuyama, Photoluminescence characteristics of YAG:Tb phosphor particles with spherical morphology and non-aggregation, J. Phys. Chem. Solids 60 (1999) 1855–1858.
[19] W.N. Wang, W. Widiyastuti, T. Ogi, I.W. Lenggoro, K. Okuyama, Correlations between crystallite/particle size and photoluminescence properties of submicrometer phosphors, Chem. Mater. 19 (7) (2007) 1723–1730.
[20] O. Milosevic, L. Mancic, M.E. Rabanal, B. Yang, P.D. Townsend, Structural and luminescence properties of Gd_2O_3:Eu^{3+} and $Y_3Al_5O_{12}$:Ce^{3+} phosphor particles synthesized via aerosol, J. Electrochem. Soc. 152 (2005) G707–G713.
[21] H. Koo, S. Ju, DS. Jung, SK. Hong, DY. Kim, YC. Kang, Morphology control of Gd_2O_3:Eu phospor particles with cubic and monoclinic phases prepared by high temperature spray pyrolysis, Jpn. J. Appl. Phys. 45 (6A) (2006) 5018–5022.
[22] J.S. Bae, S.S. Yi, J.H. Kim, K.S. Shim, B.K. Moon, J.H. Jeong, Y.S. Kim, Crystalline-phase-dependent red emission behavior of Gd_2O_3:Eu^{3+} thin-film phosphors, Appl. Phys. A 82 (2) (2006) 369–372.
[23] K.J. Batenburg, S. Bals, J. Sijbers, C. Kübel, P.A. Midgley, J.C. Hernandez, U. Kaiser, E.R. Encina, E.A. Coronado, G. Van Tendeloo, 3D imaging of nanomaterials by discrete tomography, Ultramicroscopy 109 (6) (2009) 730–740.
[24] P.F.C. Gilbert, The reconstruction of a three dimensional structure from projections and its applications to electron microscopy II Direct methods, Proc. R. Soc. London Ser. B 182 (1066) (1972) 89–102.
[25] D.S. Jung, S.B. Park, Y.C. Kang, Gd_2O_3:Eu phosphor particles prepared from spray solution containing boric acid flux and polymer precursor by spray pyrolysis, Korean J. Chem. Eng. 27 (6) (2010) 1621–1645.
[26] K. Suenaga, S. Iijima, H. Kato, H. Shinohara, Fine structure analysis of Gd M45 near egde EELS on the valence state of Gd@C82 microcrystals, Phys. Rev. B: Condens. Matter 62 (3) (2000) 1627–1630.
[27] J.A. Fortner, E.C. Back, The chemistry of the light rare-earth elements as determined by electron energy loss spectroscopy, Appl. Phys. Lett. 68 (1996) 26–29.
[28] RF. Egerton, Electron Energy-Loss in the Electron Microscope, Plenum Press, New York, 1996.
[29] T. Manoubi, C. Colliex, Quantitative EELS on M4,5-edges in rare earth oxides, J. Electron Spectrosc. Relat. Phenoma 50 (1990) 1–18.
[30] L.S. Gómez, M.E. Rabanal, J.M. Torralba, L. Mancic, O. Milosevic, Structural and morphological study of nanoceramics prepared by spray pyrolysis, Ceram. Trans. Charact. Control Interfaces High Qual. Adv. Mater. 198 (2007) 193–197.